Strongly nonlinear waves of nonplanar mode in a circular duct

Takeru Yano

Department of Mechanical Science, Faculty of Engineering, Hokkaido University, Sapporo 060, Japan

Abstract: Propagation of weak shock waves and strongly nonlinear acoustic waves of the lowest order nonplanar mode in a circular duct filled with an ideal gas is numerically investigated by using a high resolution upwind TVD scheme. The result shows that, when the nonlinearity is moderately strong and the source frequency is moderately high, the initial sinusoidal wave profile can evolve into shocks, although according to the weakly nonlinear theory a nonlinear Schrödinger equation determines the wave motion in a steady state, where a shock wave does not appear. Furthermore, strongly nonlinear waves can induce vortex-ring-like streaming jet (mean mass flow), by which the density of the gas in the neighborhood of the vortex core decreases more and more as time goes by. The resulting low-density region is not only of high vorticity but also of high entropy and high temperature.

Key words: Nonlinear acoustics, Strongly nonlinear waves, Shock waves, Shock reflection, Vortex generation, Entropy production, Streaming

1. Introduction

We shall consider the propagation of strongly nonlinear waves of the lowest order nonplanar mode in a semi-infinite circular duct filled with an ideal gas. It is assumed that the wave is radiated by a sinusoidal vibration of sound source at one end of the duct, whose frequency is comparable with but larger than the linear cutoff frequency (see Fig. 1). The nonlinear phenomena of nonplanar waves in the circular duct have been analyzed by many authors: Keller and Millman (1971) have obtained a nonlinear wavenumber shift; Nayfeh (1975) has derived a nonlinear Schrödinger equation for a complex amplitude of quasi-monochromatic wave train; Nozaki and Taniuti (1986) have shown a soliton solution for the nonlinear Schrödinger equation; Larraza and Coleman (1996) have discussed the possibility of AM–FM conversion in a quasi-monochromatic wave train. Aranha et al. (1982) have numerically examined nonlinear wave behavior near and below cutoff. Those analyses, however, are confined in a weakly nonlinear regime, i.e., they are imposed the restriction that an acoustic Mach number $M \equiv a\omega/c_0$ should be sufficiently small compared with unity, where a is the maximum amplitude of harmonic oscillation of the source, ω is an angular frequency of the oscillation, and c_0 is the speed of sound in an initial undisturbed gas. According to the weakly nonlinear theory, shock waves are not produced in a steady state because of dispersion.

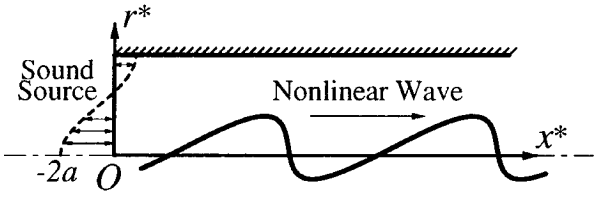

Figure 1. Schematic of the model. x^* is the distance along the axis of the duct from an initial location of sound source (cf. Eq. 10) and r^* is the distance from the axis. The sound source is a vibrating surface of angular frequency ω; the amplitude of its vibration is symmetric around the axis and varies with r^* as the Bessel function of zeroth order.

Recently, some problems of shock waves and strongly nonlinear acoustic waves have numerically been investigated by Yano and Inoue (1996a) and Yano and Inoue (1996b). They have pointed out several features forming striking contrasts to the well-known weakly nonlinear problems of $M \ll 1$. In this paper, we shall numerically examine the strongly nonlinear wave phenomenon in the circular duct, characterized by the conditions

$$M \equiv \frac{a\omega}{c_0} = O(1), \tag{1}$$

$$Re \equiv \frac{(\gamma+1)c_0 a}{\delta} \gg 1, \tag{2}$$

$$\Omega_c < \Omega \equiv \frac{R\omega}{c_0} = O(1), \tag{3}$$

where γ is the ratio of specific heats for the ideal gas, δ is the diffusivity of sound, R is the radius of the circular duct, and Ω_c is a normalized linear cutoff frequency of the lowest order nonplanar mode. The

first condition $M = O(1)$ means that the nonlinear effect is so strong that the initial smooth profile of the radiated sound may rapidly be transformed into the shock wave in the near field. The second condition $Re \gg 1$ means that we can regard the shock as a discontinuity and may ignore the dissipation effect everywhere except for the shock front (Re is referred to as an acoustic Reynolds number). The third condition signifies that the frequency at the source is comparable with but larger than the linear cutoff frequency.

Our purpose is to clarify the strongly nonlinear effect on the wave phenomenon characterized by Eqs. (1)–(3), by solving the system of axisymmetric Euler equations with a high-resolution upwind TVD finite difference scheme (Chakravarthy (1987)).

2. Formulation of the problem

We shall formulate the problem mathematically. To do so, the following nondimensional variables are introduced (see Fig. 1):

$$t = \omega t^*, \quad x = \frac{x^*\omega}{c_0}, \quad r = \frac{r^*\omega}{c_0},$$
$$u = \frac{u^*}{c_0}, \quad v = \frac{v^*}{c_0}, \quad \rho = \frac{\rho^*}{\rho_0}, \quad p = \frac{p^*}{\rho_0 c_0^2}, \tag{4}$$

where x^* is the distance along the axis of the circular duct from an initial location of sound source (see Eq. 10), r^* is the distance from the axis, u^* and v^* are respectively x^* and r^* components of the fluid velocity, ρ^* is the density of the gas, and p^* is the pressure (ρ_0 is an initial undisturbed density).

The governing equations are the Euler equations for axisymmetric flow,

$$\frac{\partial \rho}{\partial t} + \frac{\partial \rho u}{\partial x} + \frac{\partial \rho v}{\partial r} + \frac{\rho v}{r} = 0, \tag{5}$$
$$\frac{\partial \rho u}{\partial t} + \frac{\partial p + \rho u^2}{\partial x} + \frac{\partial \rho uv}{\partial r} + \frac{\rho uv}{r} = 0, \tag{6}$$
$$\frac{\partial \rho v}{\partial t} + \frac{\partial \rho uv}{\partial x} + \frac{\partial p + \rho v^2}{\partial r} + \frac{\rho v^2}{r} = 0, \tag{7}$$
$$\frac{\partial e}{\partial t} + \frac{\partial (e+p)u}{\partial x} + \frac{\partial (e+p)v}{\partial r} + \frac{(e+p)v}{r} = 0, \tag{8}$$

where $e = \rho(u^2 + v^2)/2 + p/(\gamma - 1)$ is a nondimensionalized total energy of the ideal gas per unit volume. Shock waves and contact surfaces can be represented as discontinuities in a weak solution of system (5)–(8). Condition (2) is responsible for the use of the Euler equations, as long as the boundary layer on the wall is sufficiently thin compared with a typical wavelength; we assume this and ignore the boundary layer (see also section 4.3.).

Since we want to study the lowest order nonplanar mode, we shall suppose that the boundary condition on the sound source is

$$\frac{\partial h}{\partial t} + u\frac{\partial h}{\partial x} + v\frac{\partial h}{\partial r} = 0, \tag{9}$$

on a vibrating surface prescribed by

$$h(x, r, t) \equiv x - H(t)\, M J_0\Big(j_1 \frac{r}{\Omega}\Big)(\cos t - 1) = 0, \tag{10}$$

where $H(\cdot)$ is the Heaviside unit step function, $J_0(\cdot)$ is the Bessel function of zeroth order, and $j_1 = 3.8317...$ denotes the smallest positive zero of the Bessel function of first order. Note that Ω defined in Eq. (3) also has the meaning of a nondimensionalized radius of the duct and that Ω_c is equal to j_1. The boundary condition on the side wall and a symmetry condition on the axis are

$$v = 0 \quad \text{on} \quad y = \Omega \quad \text{and} \quad y = 0. \tag{11}$$

The initial conditions at $t = 0$ are

$$u = v = 0, \quad \rho = 1, \quad p = 1/\gamma. \tag{12}$$

3. Linear and weakly nonlinear theory

In the limit of $M \to 0$, Eqs. (9) and (10) reduce to

$$u = -H(t)\, M J_0\Big(j_1 \frac{r}{\Omega}\Big) \sin t \quad \text{at} \quad x = 0. \tag{13}$$

Then, the excited wave motion can be regarded as a linear one, and it is described by a nondimensional velocity potential Φ:

$$\Phi = -H(t - x)\frac{M}{\kappa} J_0\Big(j_1 \frac{r}{\Omega}\Big)\Big[\cos(t - \kappa x) + \int_t^\infty \sin(t - \tau) J_0\Big(\frac{j_1}{\Omega}\sqrt{\tau^2 - x^2}\Big)\, d\tau\Big], \tag{14}$$

where

$$\kappa = \sqrt{1 - (j_1/\Omega)^2}\,. \tag{15}$$

Equation (15) is a normalized linear dispersion relation for the lowest order nonplanar mode. The scalar potential Φ gives $u = \partial\Phi/\partial x$, $v = \partial\Phi/\partial r$, and $p = (1/\gamma) - \partial\Phi/\partial t + O(M^2)$. The integral term in Eq. (14) denotes the initial transient effect which decays as $t^{-1/2}$. After the transient effect dies out, the wave motion reaches a steady state. The harmonic wave in the steady state has a normalized phase velocity κ^{-1} and group velocity κ.

For the case that M is sufficiently small compared with unity but finite, a weakly nonlinear theory has been established. According to the theory, the weak

nonlinear effect and dispersion effect balance in the far field in the steady state, and the wave motion there is governed by a nonlinear Schrödinger equation (Nayfeh (1975))

$$i\frac{\partial \Psi}{\partial x} + \alpha \frac{\partial^2 \Psi}{\partial \theta^2} + \beta |\Psi^2| \Psi = 0, \qquad (16)$$

where $i = \sqrt{-1}$, Ψ is a complex magnitude of quasi-monochromatic wave train, $\theta = t - (1/\kappa)x$ is a retarded time (time on the coordinate moving with the group velocity κ), $\alpha = -(1-\kappa^2)/(2\kappa^3)$, and β is a constant depending upon M and Ω, which has numerically been proved positive for all Ω ($> \Omega_c$) and M (> 0). Since both α and $-\beta$ are negative, monochromatic waves are stable and Eq. (16) has a soliton solution which is an envelope hole of quasi-monochromatic wave train. The theory claims that shock waves cannot form in the case of harmonic excitation at the source.

We shall remark that, in rectangular (or two-dimensional) ducts, the harmonic excitation at the source leads to the shock formation in the weakly nonlinear regime (Ginsberg and Miao (1986)), although the corresponding linear wave motion should satisfy a dispersion relation very similar to Eq. (15). The cause of the difference between circular and rectangular ducts may be attributed to the fact that all higher harmonics resonate in unison in rectangular ducts but not in circular ducts. However, an uncertainty still remains for the criterion of shock formation, because shock waves can be formed in a circular duct for not so large M, as we shall see in the next section.

4. Strongly nonlinear waves

We shall examine the strongly nonlinear problem of $M = O(1)$, $Re \to \infty$, and $\Omega_c < \Omega = O(1)$. To this end, the initial and boundary value problem, Eqs. (5)–(11), is numerically solved by using a high resolution TVD scheme (Chakravarthy (1987)). In the following, we shall demonstrate typical numerical results. In all computations, both Δx and Δr are set at $2\pi/160$ and $\Delta t \leq \Delta x/5$. The ratio of specific heats γ is fixed at 1.4 (air).

4.1. Formation and propagation of shock waves

Owing to the strongly nonlinear effect, the profile of the wave is rapidly distorted as the wave propagates. As shown in Fig. 2, in the case of moderately large Ω, the waveform distortion leads to the formation of shock waves with curved fronts in the near field. We shall emphasize that the shock

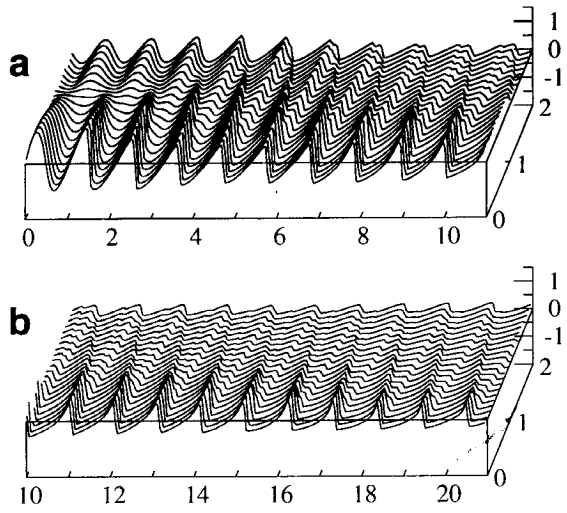

Figure 2. Wave profile of the normalized gas density $(\rho - 1)/M$ for $M = 0.1$ and $\Omega = 4\pi$ at $t = 80\pi$. The abscissa and ordinate are the distances from the source and the axis, respectively, which are normalized by $2\pi c_0/\omega$. **a**: $0 \leq x/2\pi \leq 11$, **b**: $10 \leq x/2\pi \leq 21$.

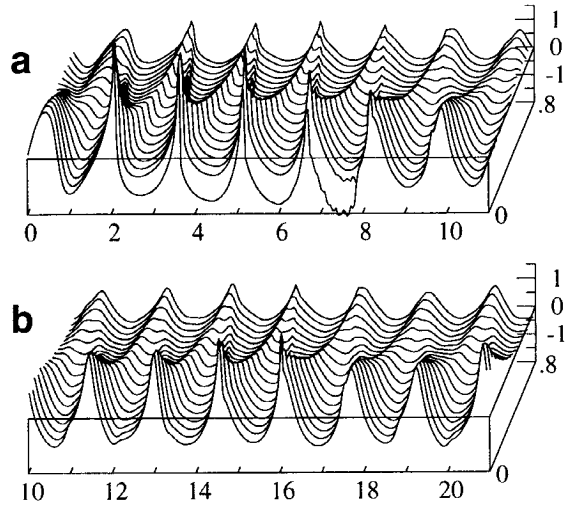

Figure 3. Wave profile of the normalized density. $M = 0.1$ and $\Omega = 8\pi/5$ at $t = 80\pi$. The abscissa and ordinate are the same as those in Fig. 2.

fronts propagate obliquely in the duct, repeatedly reflected from the wall. In Fig. 2, three shock fronts intersect at a shock triple point near the axis of the duct (see also Fig. 4**a**). Further calculation shows that the distance between the triple point and the axis decreases with decrease in Ω. When Ω is smaller than 2π, the shock intersection occurs on the axis, i.e., the triple point does not emerge. For $\Omega > 2\pi$, in the vicinity of the axis, the wave behaves as a sawtooth-like plane wave (see Fig. 2**b** and also Yano and Inoue (1996c)).

In Fig. 3, we shall present a wave profile of smaller Ω, where the shock triple points are not definitely observed (see also Fig. **4b**). In this case, as shown in Fig. **3b**, shock waves disappear in the far field although the waveform is still distorted there. Another feature in smaller Ω case is that, as shown in Fig. 3, the wave profile on the axis has spiky crests, because the focusing effect (or the interference of the waves reflected from the side wall) becomes strong with decrease in Ω.

4.2. Vorticity generation and its accumulation

In general, even if the flow field is initially irrotational, vorticity can be produced behind a curved shock front or shock of non-uniform strength along its front, as well as at a shock intersection point (Landau and Lifshitz (1987)). In the present problem, the flow field can be changed from irrotational one to rotational one after shock waves are formed. However, vorticity production behind a curved shock front is very weak compared with that at a shock triple point.

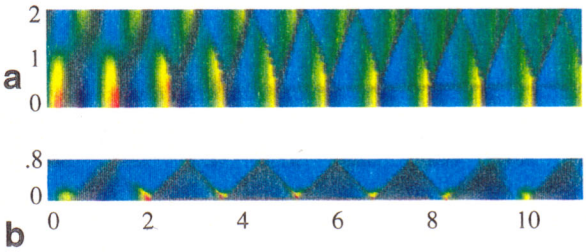

Figure 4. Gas density contour. **a**: $M = 0.1$ and $\Omega = 4\pi$ at $t = 80\pi$, **b**: $M = 0.1$ and $\Omega = 8\pi/5$ at $t = 80\pi$. The abscissa and ordinate are the same as those in Fig. 2.

In the case of moderately large Ω, the continuous harmonic excitation at the source results in the generation of a sequence of shock triple points near the axis (see Fig. 2 and Fig. **4a**). At the triple points, vorticity is strongly produced and this forms a contact surface (vortex sheet) as in the Mach reflection in supersonic flow. However, unlike the supersonic flow problem, many shock triple points are generated and they trace almost the same path, because the source motion is periodic. Consequently, vorticity is accumulated along the trajectory of triple points. Thus, it develops into a moderately strong cylindrical vortex sheet coaxial with the duct (see Fig. **4a** and also Fig. 5).

On the other hand, in the lower frequency case, as in the regular shock reflection in supersonic flow, no shock triple points appear and shock fronts may be regarded as planes (see Fig. **4b**). The flow field continues to be irrotational even after many shock waves are formed.

In Fig. 5, we shall show the evolution of the magnitude of a time-averaged vorticity defined as

$$\overline{\Omega}(x,r,t) = \frac{1}{2\pi}\int_{t-2\pi}^{t}\left(\frac{\partial v}{\partial x} - \frac{\partial u}{\partial r}\right)\mathrm{d}t. \qquad (17)$$

Clearly, the strength of vorticity on the vortex sheet increases more and more as time goes by, while vorticity elsewhere remains very weak at least until $t = 80\pi$. Note that a region from the sound source to the shock formation distance is irrotational.

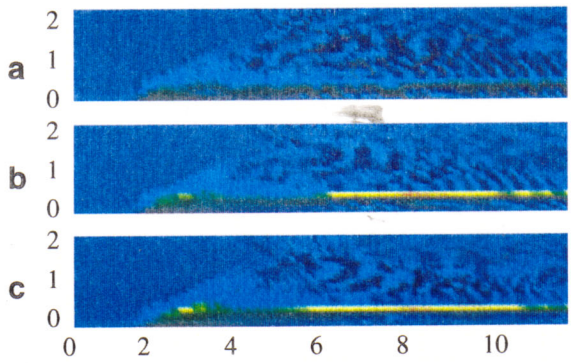

Figure 5. Time-averaged vorticity contour. $M = 0.1$ and $\Omega = 4\pi$ at $t = 80\pi$. The abscissa and ordinate are the same as those in Fig. 2. **a**: $t = 40\pi$, **b**: $t = 60\pi$, **c**: $t = 80\pi$. In **c**, the magnitude of time-averaged vorticity on the vortex sheet is about 0.02.

4.3. Evolution of vortex-ring-like streaming and jet

It is obvious that linear acoustic waves excited harmonically at the source are not accompanied by a substantial current of mass, because a time average of mass flux at any point vanishes. In a nonlinear wave field, however, even though it is excited harmonically, the substantial current can be induced. This is referred to as acoustic streaming.

In this paper, we shall define the streaming velocity by a time-averaged mass flux density vector,

$$\begin{pmatrix}\overline{m}_x(x,r,t)\\ \overline{m}_r(x,r,t)\end{pmatrix} = \frac{1}{2\pi}\int_{t-2\pi}^{t}\begin{pmatrix}\rho u\\ \rho v\end{pmatrix}\mathrm{d}t. \qquad (18)$$

In Fig. 6, we demonstrate how streaming evolves. It can be seen from the figure that a vortex-ring-like flow pattern is established in the near field. On and near the axis, the steaming motion is jet like and its velocity grows more and more as time goes by. The

vortex sheet shown in Fig. 5 may be interpreted as the shear layer which develops on the boundary of streaming jet.

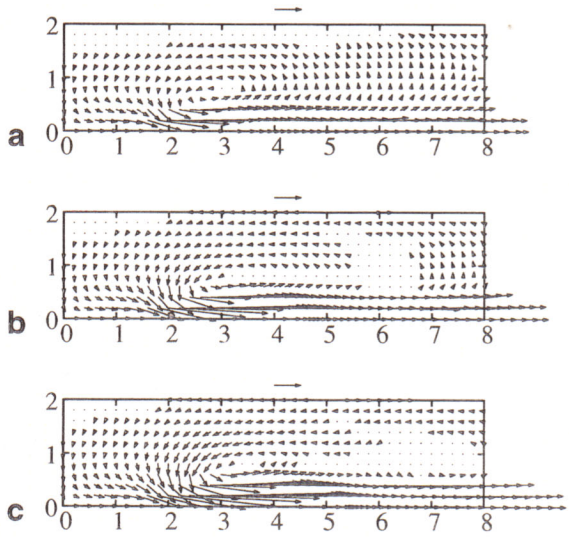

Figure 6. Time-averaged mass flux density vector for the case of $M = 0.1$ and $\Omega = 4\pi$. The abscissa and ordinate are the same as those in Fig. 2. **a**: $t = 40\pi$, **b**: $t = 60\pi$, **c**: $t = 80\pi$. An arrow of length M^2 is shown on the top of each figure for reference. The maximum magnitude of time-average mass flux density at $t = 80\pi$ is 0.054, attained at $(x/2\pi, r/2\pi) = (2.9, 0)$.

It may here be noted that in reality classical acoustic streaming may also be induced by a rotational flow in the boundary layer on the wall, which is not taken into account in the present analysis (see, e.g., a classical work by Rayleigh (1945)). The actual streaming pattern may be the superposition of classical streaming and the vortex-ring-like streaming jet. However, the magnitude of classical streaming is of $O(M^2)$ and it does not have accumulative property, namely, it is a steady flow. Therefore, with a lapse of time, the vortex-ring-like streaming jet becomes the dominant streaming motion, at least on and near the axis.

Figure 7 shows the temporal evolution of streaming jet on the axis. It seems that the maximum velocity on the axis increases with time to some limiting value. A similar streaming motion has recently been studied in a one-dimensional weakly nonlinear problem by Yano and Inoue (1996c) (see also Yano (1996)), where it has analytically been shown that a sawtooth-like plane wave causes a nonzero quasi-steady mean mass flow in the positive x direction. In the present problem, the wave profile in the vicinity of the axis can be regarded as a sawtooth-like plane wave, as shown in Figs. 2 and 4**a**. The result in the previous one-dimensional problem may therefore be used for accounting for the behavior of streaming jet: In a wave cycle of the sawtooth-like profile, the area of compression phase is larger than that of rarefaction phase because a shock front propagates with a speed slightly larger than c_0; hence the wave cycle carries an amount of gas in the positive x direction.

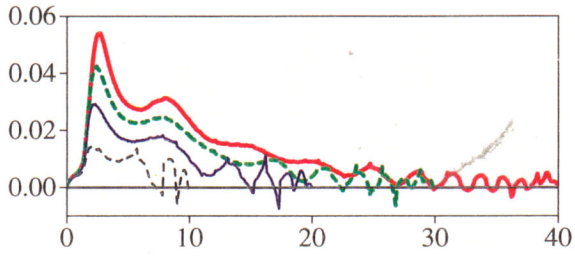

Figure 7. Distribution of velocity of streaming jet on the axis, $\overline{m}_x(x, 0, t)$, for $M = 0.1$ and $\Omega = 4\pi$. The abscissa is $x/2\pi$. Bold solid curve is at $t = 80\pi$, bold dashed curve $t = 60\pi$, thin solid curve $t = 40\pi$, and thin dashed curve $t = 20\pi$.

4.4. Formation of low-density region

In the previous one-dimensional weakly nonlinear analysis (Yano and Inoue (1996c)), it is a natural consequence that the uni-directional current of mass should cause the decrease in density in the gas. Even in the present problem, the density is gradually decreased in a region near the vortex core as shown in Fig. 8, where the distribution of a time-averaged density of the gas defined by

$$\overline{\rho}(x, r, t) = \frac{1}{2\pi} \int_{t-2\pi}^{t} \rho \, \mathrm{d}t, \tag{19}$$

is presented.

Again, the result of Yano and Inoue (1996c) is available for explaining the appearance of the low-density region in this multi-dimensional problem. According to Yano and Inoue (1996c), two effects at each shock front of sawtooth-like wave, i.e., entropy production and radiation of reflected acoustic wave of very small amplitude, reduce the density immediately behind the shock front by an amount of gas carried by the shock front (see also Yano (1996)). The effect of entropy is eight times as large as the effect of reflected acoustic wave (in normalized quantities in the air). At every time a shock passes a point in the neighborhood of the axis, the entropy at the point increases, and hence the density decreases there. As a result, a high-entropy region, i.e., low-density region, is built up in a lane of the sawtooth-like plane wave. Since the entropy

only is convected with a fluid particle, which is oscillating around an equilibrium point in the leading order of approximation, vortex-ring-like streaming cannot distribute the localized entropy. Therefore, the local depression of time-averaged density field cannot be filled up.

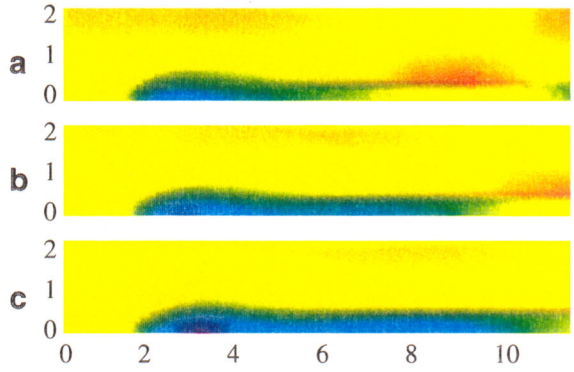

Figure 8. Evolution of the time-averaged density $\overline{\rho}$ for $M = 0.1$ and $\Omega = 4\pi$. The abscissa and ordinate are the same as those in Fig. 2. **a**: $t = 40\pi$, **b**: $t = 60\pi$, **c**: $t = 80\pi$. In **c**, the lowest time-averaged density is 0.975 at $(x/2\pi, r/2\pi) = (2.9, 0)$.

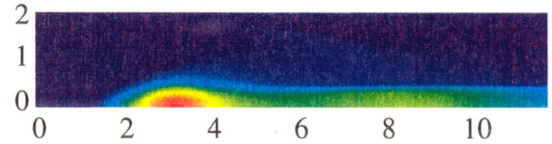

Figure 9. Distribution of entropy increment $\ln(\gamma p/\rho^{\gamma})$ for the case of $M = 0.1$ and $\Omega = 4\pi$ at $t = 80\pi$. The abscissa and ordinate are the same as those in Fig. 2. The maximum entropy increment at $t = 80\pi$ is 0.031 at $(x/2\pi, r/2\pi) = (3, 0)$.

From Figs. 5 and 8, one can see that the low-density region includes the high-vorticity region. Furthermore, the region of low density is that of high entropy as shown in Fig. 9. It also is a region of high (time-averaged) temperature.

5. Conclusions

We have numerically investigated the propagation process of weak shock waves and strongly nonlinear acoustic waves of nonplanar mode in a circular duct filled with an ideal gas. It has been shown that shock waves can be formed in the case of moderately high frequency, although in the low-frequency case shock waves disappear in the far field. In the moderately high frequency case, a sequence of shock triple points is generated and vorticity is accumulated with time on the vortex sheet. The vortex-ring-like streaming jet is excited on and near the axis. The jet decrease the density in the vicinity of the vortex core more and more as times goes by, and thus the low-density region appears. Such streaming with rarefaction effect has also been found in Yano and Inoue (1996a) and Yano and Inoue (1996b). Finally, we shall remark that streaming jet may become turbulent in the far field as suggested by Lighthill (1978) (cf. Fig. 7).

Acknowledgement. The author would like to thank Professor Yoshinori Inoue for his encouragement.

References

Aranha JA, Yue, DKP, Mei CC (1982) Nonlinear waves near a cut-off frequency in an acoustic duct—a numerical study. J Fluid Mech 121:465–485

Chakravarthy SR (1987) Development of upwind schemes for the Euler equations. NASA Contract Report 4043

Ginsberg JH, Miao HC (1986) Finite Amplitude distortion and dispersion of a nonplanar mode in a waveguide. J Acoust Soc Am 80:911–920

Keller JB, Millman MH (1971) Finite-amplitude sound wave propagation in a waveguide. J Acoust Soc Am 49:329–333

Landau LD, Lifshitz EM (1987) Fluid Mechanics 2nd edition. Pergamon

Larraza A, Coleman WF (1996) Solitons, pulse splitting, and AM–FM conversion in cylindrical ducts. J Acoust Soc Am 100:139–147

Lighthill MJ (1978) Acoustic streaming. J Sound Vib 61:391–418

Nayfeh AH (1975) Nonlinear propagation of a wave packet in a hard-walled circular duct. J Acoust Soc Am 57:803–809

Nozaki K, Taniuti T (1986) Envelope solitons in nonlinear acoustics. Physica 18D:127–134

Rayleigh JWS (1945) The Theory of Sound. Dover

Yano T (1996) Mass, momentum and total excess energy transported by a weak plane N wave. Shock Waves 6:312–322

Yano T, Inoue Y (1996a) Strongly nonlinear waves of nonplanar mode in a two-dimensional waveguide. Nonlinear Acoustics in Perspective. Nanjing University Press 159–164

Yano T, Inoue Y (1996b) Strongly nonlinear waves and streaming in the near field of a circular piston. J Acoust Soc Am 99:3353–3372

Yano T, Inoue Y (1996c) Quasisteady streaming with rarefaction effect induced by asymmetric sawtooth-like plane waves. Phys Fluids 8:2537–2551